Optica Applicata, Vol. XXIX, No. 3, 1999

Stigmatic imaging by spherical hybrid surface

JAN MASAJADA, JERZY NOWAK

Institute of Physics, Wrocław University of Technology, Wybrzeże Wyspiańskiego 27, 50–370 Wrocław, Poland.

In the paper we consider the condition for stigmatic imaging by spherical surface with deposited diffractive structure (hybrid surface). The results are verified numerically. We also present an example of fringe pattern which being deposited on plane refractive surface enables stigmatic imaging.

1. Introduction

Progress in optical manufacturing technology makes various kinds of diffractive elements more available. This results in increasing interest in their optical properties. In this paper we discuss the condition for stigmatic imaging given by single spherical surface with diffractive structure (hybrid structure). Such a condition is well known in the case of a single refractive spherical surface [1], [2] and has also been specified for plane kinoform lens [3]–[5].

In the case of refractive surface the stigmatic condition has the form

$$\frac{n}{n'}\frac{\sin u}{\sin u'} = \text{const} \tag{1}$$

where n, n' are refractive indices of the medium placed in front of and behind the refractive surface, respectively, u is an aperture angle, u' is an image angle (Fig. 1). Condition (1) imposes strict limitations on possible realization of stigmatic imaging by refractive surface. The location of source and image point must satisfy the following relations:

$$s = r\left(1+\frac{n}{n'}\right), \tag{2}$$

$$s' = r\left(1+\frac{n}{n'}\right) \tag{3}$$

where s, s' are source and image z-coordinates, respectively (Fig. 1). There are two more possibilities to get stigmatic image: $-s' = -s = -r$ and $s = s' = 0$, however, they are obvious.

From the above formulas we can notice that it is impossible to get real stigmatic image of a real object with single refractive surface. The spherical hybrid surface is more flexible. One can find the fringe geometry that provides stigmatic imaging for

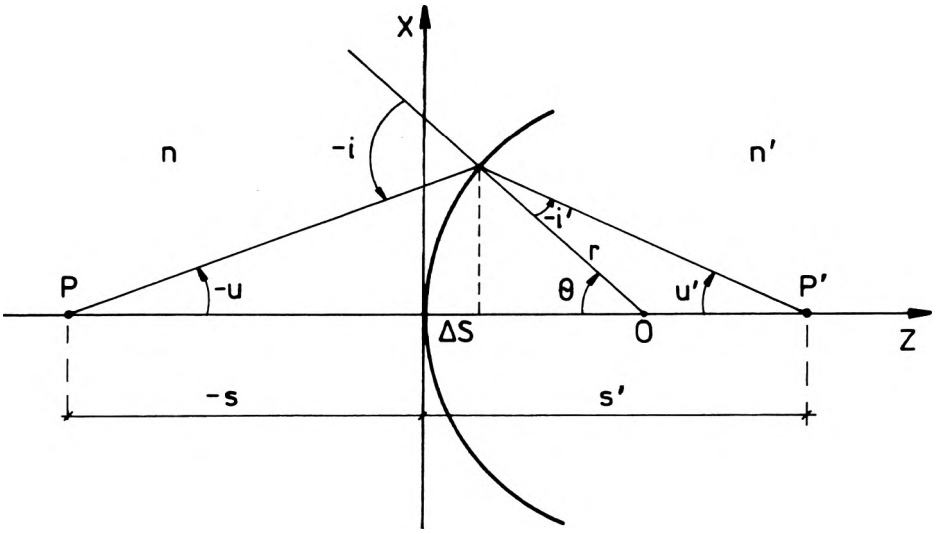

Fig. 1. Beam passing through spherical surface with an object P being at finite location.

any two points on axis. In the present paper, formulas describing such fringe geometry are derived. The diffractive structure is represented here holographically, *i.e.*, by means of two forming beams located on the optical axis (we limit our consideration to the rotationally symmetric case). This allows us to refer directly to the formula describing beam deflection at the diffraction surface (see Eq. (5)). Such representation is also intuitive, which is helpful in the system analyses. On the other hand, the formulas presented in the paper can be easily transformed to other methods of diffraction structure representation (*e.g.*, polynomial representation).

2. Ray deflection by hybrid imaging surface

In this section, we derive a formula describing the deflection of a single ray by hybrid imaging surface. We refer to the Snell refraction law and the appropriate formula describing the beam deflection by diffractive structure. The Snell refractive law may be written as

$$n'\vec{n}\times\vec{r}'_r = n\vec{n}\vec{r}_r \tag{4}$$

where $\vec{r}'_r$, $\vec{r}_r$ are unit vectors along image and object beams, respectively, $\vec{n}$ is a unit vector along the normal at the point of ray incidence.

In the case of diffractive surface the formula for the diffracted rays may be written as (Fig. 2), [6], [7]

$$\vec{n}\times\vec{r}'_d = \vec{n}\times(\vec{r}_d+\mu(\vec{r}_\alpha+\vec{r}_\beta)) \tag{5}$$

where: $\vec{r}'_d$, $\vec{r}_d$ are unit vectors along the image and object beams, $\vec{r}_\alpha$, $\vec{r}_\beta$ are unit vectors along forming beams, $\vec{n}$ is a unit vector along the local normal at the point of incidence, μ is the parameter which in holography takes the form [8]

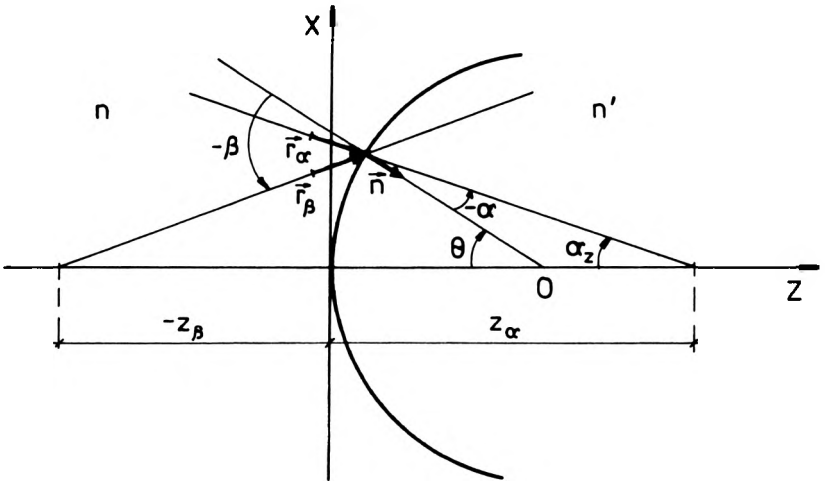

Fig. 2. Beams forming the diffractive structure.

$$\mu = \frac{\lambda_1}{\lambda_2} \tag{6}$$

λ_1 is the readout wavelength, λ_2 is the forming wavelength. Furthermore we put $\mu = 1$.

Formula (5) is valid for the primary image. For the secondary image, a plus sign in front of parameter μ must be changed to a minus sign. The diffractive structure changes the direction of the incident beam. Next, the diffracted beam can be treated as being refracted at the surface considered. Thus $\vec{r}'_d = \vec{r}_r$ and combining (4) and (5) we get

$$\vec{n} \times \vec{r}' = \frac{n}{n'} \vec{n} [\vec{r} + \mu(\vec{r}_\alpha - \vec{r}_\beta)] \tag{7}$$

where $\vec{r}' = \vec{r}'_r$ and $\vec{r} = \vec{r}_d$. In paper [9], formula (7) is derived directly from Fermat principle.

Next, we limit our considerations to the two-dimensional case. In Cartesian co-ordinates equation (7) has the form

$$\sin(-i') = \frac{n}{n'} [\sin(-i) + \sin(-\alpha) - \sin(-\beta)]. \tag{8}$$

Equation (8) my be considered as a two-dimensional refraction law for single hybrid surfaces.

3. Stigmatic imaging for finite object location

In this section, we derive a formula describing fringe geometry supporting stigmatic imaging in the case of finite location of the object. From Fig. 1 we can find the following geometrical relations:

$$r-s = r\frac{\sin(-i)}{\sin(-u)}, \tag{9}$$

$$s'-r = r\frac{\sin(-i')}{\sin(u')}. \tag{10}$$

Dividing Equations (10) and (9) and combining the result and Eq. (8) we get

$$\frac{r-s'}{r-s} = \frac{n}{n'}\frac{\sin(-i)+\sin(-\alpha)-\sin(-\beta)}{\sin i}\frac{\sin u}{\sin u'}. \tag{11}$$

For a spherical surface the value of angle α is

$$-\alpha = \Theta-\alpha_z \tag{12}$$

where α_z is an angle between forming beam r_α and optical axis z. Angle i is equal to (Fig. 1)

$$-i = \Theta-u. \tag{13}$$

Combining (11), (12) and (13) we get

$$\frac{r-s'}{r-s} = \frac{n}{n'}\frac{\sin(\alpha_z-\Theta)+\sin(-\alpha)-\sin(-\beta)}{\sin(u-\Theta)}\frac{\sin(u)}{\sin(u')}. \tag{14}$$

In order to get the stigmatic imaging condition we have to eliminate u' from the above equation. From Fig. 1 we have

$$\tan(u') = \frac{z}{z'}\tan(u) \tag{15}$$

where: $z = -s+\Delta s$ and $z' = s'-\Delta s$.

Taking (15) into (14) we get

$$\alpha_z = \arcsin\left\{\frac{r-s'}{r-s}\frac{n'}{n}\frac{\sin[\arctan(z/z'\tan(u))]}{\sin(u)}\sin(\Theta-u)-\sin(-\alpha)+\sin(-\beta)\right\}+\Theta. \tag{16}$$

Following the holographic reconstruction scheme (the object is located at the position of one of the forming beams: $-s = -z_\beta$, hance $-i = -\beta$ (Figs. 1 and 2)) we can simplify Eq. (16) to the form

$$\alpha_z = \arcsin\left\{\frac{r-s'}{r-s}\frac{n'}{n}\frac{\sin[\arctan(z/z'\tan(u))]}{\sin(u)}\sin(\Theta-u)\right\}+\Theta. \tag{17}$$

It is worth noting that for the plane surface Eq. (16) takes the form

$$\alpha_z = \arcsin\left\{\frac{n'}{n}\frac{\sin(\arctan(z/z')\tan(u))}{\sin(u)}\right\}. \tag{18}$$

The values of angle α_z calculated from Eqs. (16)–(18) result in different locations of the forming beam z_α for varying aperture angle u (Fig. 2). This makes it impossible to record the appropriate diffractive structure in the holographic way. However, for each aperture angle we can use Eqs. (16)–(18) to find the corresponding location z_α. Next, we can calculate the phase shift Φ_u introduced by the corresponding diffractive structure

$$\Phi_u = \Phi_\alpha - \Phi_\beta \tag{19}$$

where

$$\Phi_q = \frac{2\pi}{\lambda_2} R_q \tag{20}$$

with R_q being an optical path length from the source point z_q to the point of beam intersection. Next, we can plot the diffractive structure (corrected diffractive structure) using one of the computer-aided methods.

4. Stigmatic imaging for infinite object location

Equations (16)–(18) have different form when the object is located at infinity (plane wave illumination). From Fig. 3 we can find:

$$u' = \arctan\left(\frac{x}{z'}\right), \tag{21}$$

$$i' = u' - \Theta, \tag{22}$$

$$-i = \Theta. \tag{23}$$

Combining the above equations and Eq. (8) we get

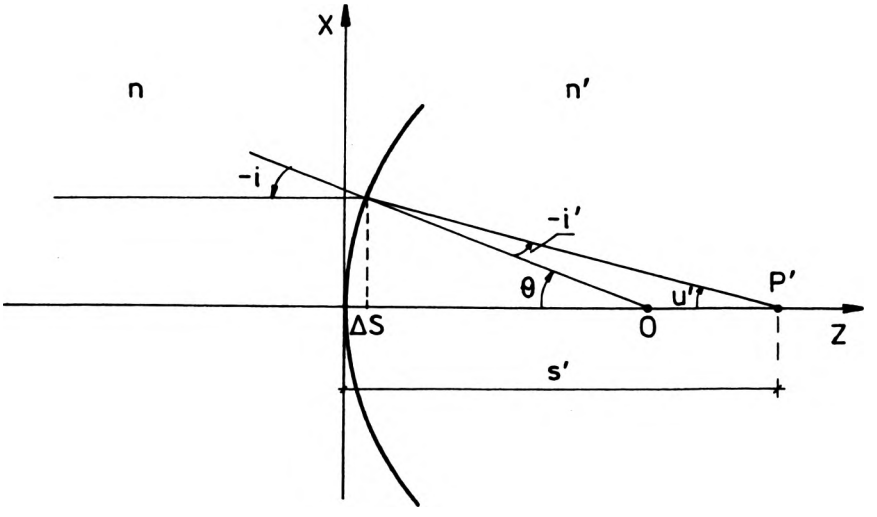

Fig. 3. Beam passing through spherical surface with an object being at infinity.

$$\sin\left(\arctan\left(\frac{x}{z'}\right)-\Theta\right)=\frac{n}{n'}[\sin(\Theta)+\sin(-\alpha)-\sin(-\beta)]. \tag{24}$$

Taking similar steps as in the previous section we get

$$\alpha_z=\arcsin\left\{\frac{n'}{n}\sin\left(\Theta-\arctan\left(\frac{x}{z'}\right)\right)+\sin(\Theta)-\sin(-\beta)\right\}+\Theta. \tag{25}$$

If we apply the holographic reconstruction scheme, Eq. (25) takes the form

$$\alpha_z=\arcsin\left\{\frac{n'}{n}\sin\left(\Theta-\arctan\left(\frac{x}{z'}\right)\right)\right\}+\Theta. \tag{26}$$

For the plane hybrid surface Eq. (25) simplifies to

$$\alpha_z=\arcsin\left\{\frac{n'}{n}\sin\left(\arctan\left(\frac{x}{z'}\right)\right)-\sin(-\beta)\right\}. \tag{27}$$

We can use Eqs. (25)–(27) to calculate the fringe geometry supporting stigmatic imaging in the same way as in Sect. 3.

5. Numerical examples

In this section, we verify numerically the results discussed in the previous sections [10], [11]. The table shows the parameters of the spherical hybrid surfaces being investigated (with radius $r = 100$ mm). The last three columns show the values of standard deviation of the aberration spot calculated for the field angles of 0, 0.02, 0.05 (in radians), respectively. The diffractive structure of hybrid surface I is designed in a standard way. In the case of hybrid surfaces II–V the corrected diffractive structures were calculated using an equation whose number is shown in the fourth column of the table. The image distance s' of hybrid surface I was calculated from paraxial optics formulas. In the case of hybrid surfaces II–V it was an arbitrary value. For the fixed image position the proper corrected diffractive structures were calculated (Eqs. (17) and (26)).

Table. Parameters and standard deviation rms of the aberration spot for the investigated spherical hybrid surfaces. The standard deviation is given in [mm]·10^{-4}. All hybrid surfaces have radius $r = 100$ mm.

No.	$z_c = s$ [mm]	$z_i = s'$ [mm]	z_α [mm]	z_β [mm]	Radius [mm]	Angle 0 rms	Angle 0.02 rms	Angle 0.05 rms
I	−50	−150	−66.66	−50	100	15.98	18.03	30.58
II	−50	−150	Eq. (17)	−50	100	0	7.47	2.14
III	−∞	−150	Eq. (26)	−400	100	0	1.71	4.73
IV	−∞	−150	Eq. (26)	−∞	100	0	1.71	4.73
V	−100	−100	Eq. (17)	−100	100	0	0.08	0.5

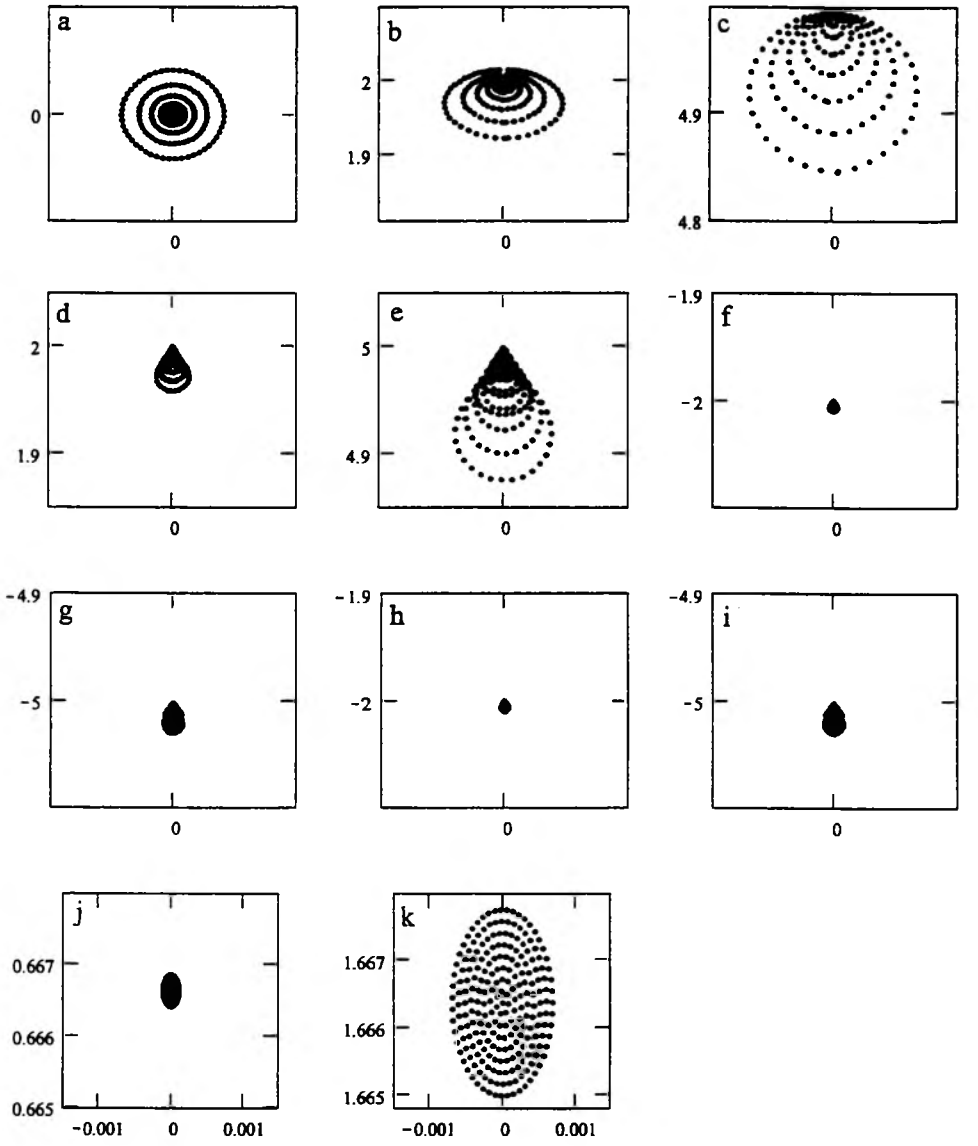

Fig. 4. Spot-diagrams for hybrid surfaces listed in the table. (**a**—**c**) hybrid surface I, field angles 0, 0.02, 0.03, (**d**, **e**) hybrid surface II, field angles 0.02, 0.04, (**f**, **g**) hybrid surface III, field angles 0.02, 0.04, (**h**, **i**) hybrid surface IV, field angles 0.02, 0.04, (**j**, **k**) hybrid surface V, field angles 0.02, 0.04.

Figures 4**a**—**k** show spot-diagrams corresponding to hybrid surfaces listed in the table. We have not included spot-diagrams for the field angle 0 in the case of hybrid surfaces II—V. In this case the imaging is stigmatic. All figures, except 4**j**, **k** are plotted to the same scale.

Comparing the spot-diagrams for hybrid surfaces I (Fig. 4**a**—**c**) and II (Fig. 4**d**, **e**) we can see that hybrid surface II with corrected diffractive structure gives better

image quality, particularly for small field angles. For larger field angles the differences become negligible. Hybrid surfaces III (Fig. 4 **f**, **g**) and IV (Fig. 4**h**, **i**) are illuminated with plane wave (infinite object location). The two hybrid surfaces differ in location of the forming source z_β. However, their aberration spots are practically the same. Studying similar cases we arrive at the same conclusion. The aberration spots do not depend on the forming source location. The last example illustrates the advantage of representing the diffractive structure in a holographic way. Following the holographic readout scheme we can easily find the location of sources that result in a diffractive structure which works as a filter compensating the refractive power of the hybrid surface ($z_\beta = z_c = z_i$). In this case, the rays originating from the object source point are not deflected at the hybrid surface. We can see that for non-zero field angles the aberration spot is very small and coma free (Figs. 4**j**, **k**) are plotted to a much smaller scale than the previous one).

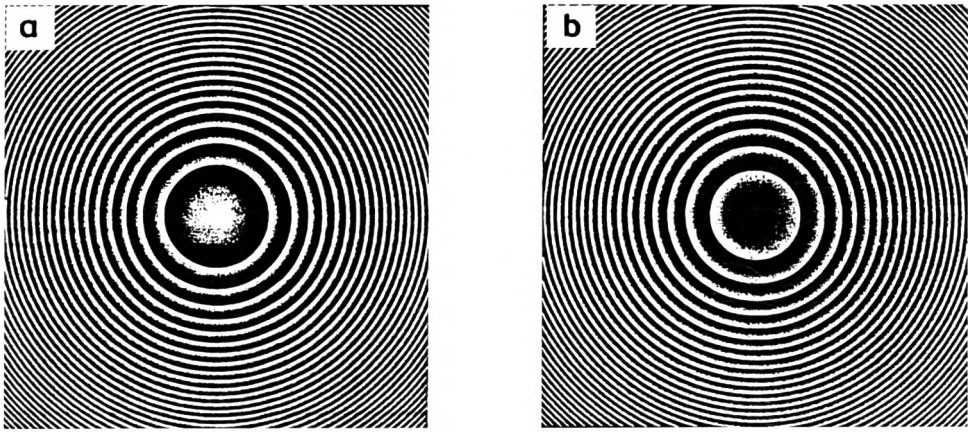

Fig. 5. Fringe pattern of plane hybrid surface with classical diffractive structure (**a**), plane hybrid surfcae with corrected diffractive structure (**b**).

Figures 5**a**, **b** show examples of diffractive structures for classical plane hybrid surfaces with source locations $z_\alpha = z_i = -150$ mm, $z_\beta = z_c = -50$ mm, and plane hybrid surface with corrected diffractive structure calculated using Eq. (19), (source location: $z_i = -150$ mm, $z_\beta = z_c = -50$ mm). Both structures were calculated and plotted by means of computer method [12], [13].

6. Conclusions

We have shown that for spherical hybrid surfaces it is possible to design the diffractive structure that yields stigmatic imaging between any two points on the axis. Although we represent the diffractive structures in a holographic way, the calculated fringe geometry cannot be realised by means of optical holography. This is not a disadvantage of the holographic approach. We can easily compute the phase shift introduced by diffractive structure and plot the desired fringe pattern. On the

other hand, the holographic approach seems to be intuitive. This allowed us to design the diffractive structure which works as a filter compensating refractive power of the hybrid system (position V in the table).

We have not discussed the problem of diffraction efficiency of the diffractive part of hybrid surface. This question is strictly related to limitations of the available technology and is not a subject matter of this paper.

References

[1] BORN M., WOLF E., *Principles of Optics*, Pergamon Press, Oxford 1991, Chap. IV.
[2] FINCHAM W. H. A., FREEMAN M. H., *Optics*, Butterworths, London 1974, Chap. XVIII.
[3] HAZARA L. N., HAN Y., DELISLE C., Opt. Commun. **91** (1992), 1.
[4] HAZARA L. N., HAN Y., DELISLE C., Opt. Eng. **34** (1995), 1296.
[5] HAZARA L. N., HAN Y., DELISLE C., Opt. Commun. **94** (1994), 203.
[6] SMITH R. W., Opt. Commun. **23** (1977), 106.
[7] WELFORD W. T., *Aberrations of Optical Systems*, Adam Hilger, Bristol, 1989.
[8] COLLIER R., BURKHARDT C., LIN L., *Optical Holography*, Academic, New York 1991, Chap. III.
[9] TWARDOWSKI P. J., HARTHONG J., J. Opt. Soc. Am. A **14** (1997), 1293.
[10] SPENCER G. H., MURTY M. V. K., J. Opt. Soc. Am. **52** (1962), 672.
[11] SMITH R. N., Opt. Commun. **55** (1985), 11.
[12] LEE W. H., *Computer-Generated Holograms: Techniques and Applications*, [In] *Progress in Optics*, Vol. 16, [Ed.] E. Wolf, North-Holland, Amsterdam 1978, p. 121.
[13] BERNARD E., J. Opt. Soc. Am. A **5** (1988), 1803.

Received July 20, 1998
in revised form December 20, 1998